HHS Public Access

Author manuscript

Ocul Surf. Author manuscript; available in PMC 2022 January 01.

Published in final edited form as:

Ocul Surf. 2021 January ; 19: 53–62. doi:10.1016/j.jtos.2020.11.008.

Creation and grading of experimental corneal scars in mice models

Devon Cogswell[a], **Mei Sun**[a], **Erin Greenberg**[a], **Curtis E. Margo**[a,c], **Edgar M. Espana**[a,b,*]

[a]From the Cornea, External Disease Service, Department of Ophthalmology, University of South Florida, Tampa, FL, USA

[b]Molecular Pharmacology and Physiology, University of South Florida, Tampa, FL, USA

[c]Pathology and Cell Biology, Morsani College of Medicine, University of South Florida, Tampa, FL, USA

Abstract

Purpose: To develop a stromal wound healing model and a reliable scar classification score system that correlates photographic evaluation with changes in the structure and organization of the extracellular matrix.

Materials and methods: We tested three stromal injury techniques in adult C57BL/6 mice. Technique 1, a lineal partial thickness keratotomy in the horizontal axis. Technique 2, corneal epithelial and stromal debridement using a diamond burr in the horizontal axis, and technique 3, a combination of techniques 1 and 2. To assess intra-observer and inter-observer agreement between two examiners evaluating formed stromal scars, stereo microscopic photographs of anterior segment were scored by two masked examiners at around 1-month. Depending on the severity of opacification and the area of involvement, scars were classified on a scale from 0 to 3 based on a modified Fantes haze scale. Extracellular matrix composition as well as matrix organization, macrophage infiltration and neovascularization were evaluated with immunofluorescence and second harmonic generation (SHG) microscopy.

Results: Technique 1 created mild scars, with a score of 0.5 ± 0.43, while techniques 2 (score 2.1 ± 0.45) and 3 (score 2 ± 0.66), created dense scars with a higher score. A significant difference in scar severity score was noted between the 3 techniques (one way ANOVA, $p < 0.0001$). Masked graders demonstrated excellent agreement (intraclass correlation = 0.927 [95% confidence interval: 0.87–0.96]). The severity of scars noted at stereo microscopy correlated with the severity of changes in extracellular matrix in the stroma as demonstrated by the expression of collagens I, IV and fibronectin and evaluation of matrix hierarchical organization. In contrast to mild scarring, moderate and severe scars had increased expression of CD31 and CD68, markers of vascular endothelial cells and macrophages, respectively.

*Corresponding author. Department of Ophthalmology, University of South Florida Morsani College of Medicine, 13330 USF Laurel Dr, 4th floor, MDC11, Tampa, FL, 33612, USA. edgarespanamd@gmail.com (E.M. Espana).

Declaration of competing interest

None of the authors in this manuscript has any conflict of interest to disclose.

Conclusion: Mouse models of stromal scarring using simple surgical techniques are described. Corneal scars can be consistently classified by two observers. Grading of scar severity positively correlates with changes in extracellular matrix composition, disorganization and cell infiltration.

Keywords

scar; Stroma; Fibroblasts; Wound; Macrophages

Introduction

The unique structure and organization of the corneal extracellular matrix (ECM) contributes to its clarity [1-4]. The stroma comprises 90% of the cornea and is made of water, collagens and proteoglycans [1-4]. Light scattering in the cornea is minimized by a highly organized arrangement of collagen fibrils combined with tightly regulated stromal hydration [1,5]. Stromal structure and function is not only dependent on ECM, it also has a cellular component. Between the orthogonal layers of collagen fibrils are a network of keratocytes, neural crest derived cells that exist in a mitotically quiescent state [6].

Significant stromal scars secondary to trauma, surgical procedures or infections commonly necessitate corneal transplantation [7]. Interventions that prevent or decrease stromal scar formation would potentially reduce the need for corneal transplantation. Before therapies to ameliorate scar formation can be fully realized, however, different animal models of stromal scarring are needed. A priority in such research includes understanding regulators in wound healing: cellular response, cytokines and extracellular matrix proteins. Mice injury models to study the function of growth factors and ECM components in corneal wound healing would be valuable. Murine extracellular matrix proteins can be manipulated genetically, mice are suitable for controlled surgery, and a variety of established anti-mouse antibodies are commercially available.

Multiple corneal injury models in mice have been reported in the literature [8]. These injury models simulate corneal scarring seen after injuries by chemical burns, penetrating incisional wounds, or laser ablation. The subject has been reviewed [8]. In general, mechanisms of trauma as well as severity of injuries vary greatly. Severe corneal injuries commonly present with a combination of traumatic penetrating or nonpenetrating laceration(s) accompanied by loss of stromal tissue or surface abrasive damage. This combined-mechanism injury can be simulated with a model that combines a partial thickness laceration and stromal abrasive injuries.

Second harmonic generation (SHG) microscopy enables contrast imaging of biological structures containing collagen [9,10]. In the cornea, SHG imaging is helpful in evaluating collagen fibril and lamellae organization. It is also valuable in evaluating the unique hierarchical organization of the corneal stroma and the process of wound healing [11-13]. Hochheimer was the first to show SHG signals could be detected in the cornea using a pulsed YAG laser [14].

In this study, we evaluate 3 different surgical techniques that created stromal scars. After creating stromal scars, we studied a panel of matrix proteins known to be important during

wound healing: collagen I, (Col I) [15], the main component of collagen fibrils, collagen IV, (Col IV), a basement membrane component that is also expressed by injured stromal fibroblasts [16]. Fibronectin (Fn), a provisional matrix component, expressed by stromal fibroblasts during early and active wound healing [17]. Biglycan, a marker of scar tissue formation [18]. CD31, a marker for endothelial cell intercellular junctions [19]. CD68, a monocyte – macrophage marker [20], and α-SMA (smooth muscle actin), a marker for myofibroblasts [21,22]. Our findings are described.

Materials and Methods

Evaluation of stromal scar formation severity created by lineal keratotomy and debridement

We evaluated three different surgical techniques. The first was a limbus-to-limbus lineal stromal keratotomy created with a custom-made diamond blade. This blade was unable to cut at more than 70 μm depth (Fig. 1). The second technique consisted of abrading trauma in the entire horizontal axis that created stromal injury. The third method was a combination of limbus-to-limbus lineal stromal keratotomy and abrasion on the sides of the lineal keratotomy for a total of 3 different techniques (Fig. 2A, B and C). The purpose of trying different surgical techniques was to simulate the type of complex injury seen in clinical practice that disrupts basement membrane and at the same time alters the tensile strength of the corneal stroma by creating a deep stromal cut. At least 8 mice were evaluated per surgical technique after power analysis calculation to obtain statistical significance. Only left corneas were injured. All experiments conformed to the use of Laboratory Animals and ARVO statement for the Use of Animals in Ophthalmic and Vision Research and were approved by the Institutional Animal Care and Use Committee of the University of South Florida College of Medicine. Adult, 60-days-old male C57BL/6 mice were anesthetized by intraperitoneal injection of ketamine (50 mg/kg) and xylazine (10 mg/kg). Once the mouse was under general anesthesia, 0.1 ml of 0.5% proparacaine hydrochloride was added to the ocular surface. Subcutaneous analgesia was given. Under microscope visualization, a partial thickness corneal laceration was performed from limbus to limbus using a custom-made diamond blade with a 70 μm guarded depth (Mastel, Rapid City, SD, USA), (Fig. 1, top). The stromal partial thickness laceration was completed in the horizontal axis of the eye. The epithelial surface was debrided with an AlgerBrush II (The Alger Company, Lago Vista, TX) until the epithelial layer was removed. Next, the diamond burr was applied to the stromal surface in 2 double passes with light pressure and visible abrasion without indentation on the cornea. Immediately after the procedure, drops of ofloxacin were applied to the ocular surface.

Scar density masked grading and intra- and inter observer agreement

Photographs were obtained using a standardized protocol. Two light sources were positioned to avoid reflections. One light source was placed at 12 o'clock and the second at 6 o'clock to enhance visualization of haze. The light sources were placed on the plane of the limbus. Two masked examiners (fellowship trained cornea specialists) classified the severity of scars, based on printed standardized photograph (i.e. standardized template). Photographs were evaluated twice in a randomized and masked manner by both observers with a one-week

interval. Depending on the severity of opacification and the area of involvement, scars were classified on a scale from 0 to 3 based on a modified Fantes haze scale, with 3 being the most severe, see Table 1 for a description of modified Fantes scale [23-26]. Twenty-five eyes were evaluated based on 80% power to detect an intraclass correlation of 0.95 and type 1 error of 0.05.

Immunofluorescence microscopy

Evaluation of different ECM proteins was studied by immunofluorescence microscopy as previously described [27]. Corneal tissue from mice at 3–4 weeks post injury was examined. Briefly, corneas were embedded and frozen in OCT medium (Sakura Finetek, Torrance, CA). Cross sections of 6 μm were cut using an NX 50 cryostat followed by immunofluorescence localization. Sections were blocked in 10% donkey serum (Sigma-Aldrich, St. Louis, MO) and then incubated overnight at 4 °C in anti-collagen IV (Southern Biotech, Birmingham, Al), anti-collagen I (Millipore, Danvers, MA), anti-fibronectin, anti-α-SMA (Abcam, Cambridge, MA), anti-biglycan antibody (a gift from Dr Larry Fisher, National Institute of health), anti-CD31 and anti-CD68 antibodies (Biolegend, San Diego, Ca) followed by Alexa Fluor 488 nm-fluorescein conjugated and 594 nm-rhodamine conjugated secondary antibodies (Molecular Probes, Eugene, OR). Positive and negative controls were processed in the same manner. The nuclei were counter-stained using Vectashield mounting solution with DAPI (Vector Lab Inc., Burlingame, CA). Images were captured using a fluorescence microscope with appropriate filters (Leica Microscopes, Germany).

Second Harmonic Generation Microscopy of Corneal Scars of Different Severity.

Enucleated eyes were immediately processed and mounted as noted above. Corneal cross sections were imaged using an Olympus MPE-RS microscope using a 25X (0.95 NA) water-immersion objective (Olympus). Two-photon SHG signals were generated using a mode-locked titanium:sapphire laser at 960 nm. The SHG forward-scattered signals passing through the corneal sections were collected using a 0.8 NA condenser lens with a narrow band-pass filter (465–485 nm). Backward-scattered SHG signals were detected with a band pass filter (460–500 nm). All samples were scanned using a 2 μm *z*-axis step size from the back to the front of the section. The two-photon excited fluorescent signals from propidium iodine was captured with a band pass filter (575–630 nm).

Statistical analysis

The data were analyzed by the Biostatistics Core at the Morsani College of Medicine, University of South Florida. Data were provided in an Excel data sheet format (Microsoft, Redmond, WA, USA). One-way ANOVA test was used to calculate statistical significance between the scar generated by three surgical techniques (GraphPad Prism 5.0; GraphPad Software, Inc., San Diego, CA, USA). Statistical power calculation was performed using IBM SPSS version 25 (IBM, Armonk, NY, USA).

Results

Stromal injury created by tissue abrasion and debridement creates scarring

Scar formation in the mouse stroma varied according to the surgical technique used (Fig. 2). We examined the corneal stroma 3–4 weeks after injury in the three injury techniques as shown in Fig. 2, using a stereomicroscope. A limbus-to-limbus lineal stromal keratotomy, technique 1, created with a custom-made diamond blade created light scars of no clinical significance or no visible scars at examination with stereomicroscope (Fig. 2D and G). Evaluation of stromal scar photographs comparing stromal abrasion caused by rotating burr (technique 2, Fig. 2E and H) to the combined technique of partial lineal stromal cut followed by stromal abrasion caused by rotating burr (technique 3) showed no apparent differences at examination (Fig. 2F and I) [23-26]. A score of 2.1 ± 0.45 was given to technique 2 and a score of 2 ± 0.66 was given to technique 3. There was statistically significant difference in the scar grading between the three techniques, one way ANOVA ($p < 0.0001$), Fig. 3.

Photographic evaluation of scar formation and agreement in grading severity between two observers

We evaluated 25 corneas of 25 mice with different grades of injury. Photographs of corneal scars were evaluated ~4 weeks post injury. There were no significant differences between subjective interpretations of repeated images with agreement for the individual with measurements obtained 1 week apart. There was excellent intra-observer agreement (intra-class correlation = 0.927 [95% confidence interval (CI): 0.87–0.96]). There was also excellent inter-observer agreement (inter-class correlation = 0.93 [95% confidence interval (CI): 0.87–0.96]) between 2 observers. These results show that two examiners agree in their assessment of stromal scar photographs in a reproducible manner and suggest that photographic assessment of stromal scars is a valid method for scar grading.

Immunohistological evaluation of scar formation and neovascularization

In order to better characterize the severity and characteristics of stromal scars, we performed immune-marker studies with fluorescence microscopy in a normal uninjured control specimen (Fig. 4) and in 3 different samples with different degrees of scar severity as just classified in agreement by the 2 observers. Mild density scars showed minimal tissue disruption, minimal macrophage infiltration and no stromal neovascularization. A well-formed and mature scar displayed no or minimal provisional matrix, demonstrated by absent fibronectin expression (Fig. 5). Moderate density scars, were characterized by significant tissue disruption, more disorganization in the extracellular matrix, significant macrophage infiltration and stromal neovascularization (Fig. 6). Finally, characterization of dense scar showed severe tissue disruption with presence of provisional matrix suggestive of continuous matrix remodeling, severe disorganization of extracellular matrix, and very dense macrophage infiltration. Stromal neovascularization was shown by collagens IV staining of blood vessels basement membrane and CD31 expression (Fig. 7). Taken together, these data show correlation between the severity of stromal scarring noted at stereo microscopy and the degree of extracellular matrix disorganization found with immunohistological markers, see Table 1.

Corneal stromal hierarchical organization and fibrillogenesis assessment by second harmonic generation

To evaluate stromal scars including hierarchical organization and fibrillogenesis, we performed SHG imaging with forward and backscattering settings in different samples with the degrees of scar severity as classified above, (Fig. 8). Throughout the stroma, normal control eyes showed distinct pattern organized into well-organized structures like lamellae that were well aligned and parallel to the epithelial layer and Descemet's membrane. Flat keratocyte nuclei were also well aligned between lamellae. Backscattered SHG signals appeared mild and diffuse without any localized area of increased signaling. A Grade 0 scar, not clinically apparent at stereo photographs, displayed disruption of fibrils and loss of lamellae organization localized to the subepithelial region of the anterior stroma. Grade 1 scars were characterized by matrix disorganization in the anterior 1/3 of the stroma. Loss of lamellae orientation and a mild increased in cell density. Minimal to no backscattering signal was noted. Finally, characterization of dense scars showed very severe tissue disruption with presence of continuous matrix remodeling, severe disorganization of extracellular matrix, and significant cell infiltration and disorganization. Stromal neovascularization was severe and worst in scars Grade 3. Taken together, these data show correlation between the severity of stromal scarring noted at stereo microscopy and the loss of hierarchical organization after injury as shown by SHG imaging.

Discussion

Genetically manipulated mice are commonly used to study biological processes. Their genes can be manipulated including so-called humanized mice that carry inserted human genes. An injury technique that consistently creates significant stromal scars in mice will complement the current techniques used that apply chemical injuries and laser ablation in the study of stromal trauma and wound healing. This is particularly relevant for research using transgenic mice and novel pharmaceutical compounds.

The quantification of corneal opacity severity has some subjectivity and is dependent on several variables. The use of photographic and histological evaluation has the advantage of simplicity but modern corneal imaging techniques like in vivo confocal microscopy and optical coherence tomography of the anterior segment are very helpful in objectively characterizing formed scars in terms of scar depth, size and density [18,28]. Photographic imaging is advantageous when multiple experienced observers cannot be present at the same time and place. In vivo examination and grading of corneal opacities can be easily done using a standardized illumination technique. However, mouse heart beat and unintentional mouse movements can preclude the acquisition of high quality photographs. We have commonly taken photographs with live mice and with mice under general anesthesia to evaluate and grade corneal scarring using our grading scale, but the rapid development of cataracts after anesthesia induction hinders interpretation. Our results show that evaluation of scar tissue by the same observer on two different occasions and by two different observers on two different occasions had a high percentage of agreement. Photographic evaluation by experienced observers appears to be a valid method to asses and grade scar formation in mice corneas.

The formation of stromal scars in the mouse, compared to other mammal models (e.g. primates and rabbits), is unique due to biological factors like reduced keratocyte transformation to myofibroblasts that is noted even in the presence of significant matrix disorganization [29]. The mouse stroma following injury is rarely populated by α-SMA positive myofibroblast, a cell type that plays a major role in scar formation in other mammals, and a cell type that is considered the hallmark of scar formation [29,30]. We allowed ~4 weeks post injury before evaluating scar formation, based on previous reports that established this time as optimal in mice [18,30]. Interestingly, we did not find myofibroblasts in scars grades 0 and 1 and the expression was very mild in scars grade 2. In contrast, we found that dense and vascularized scars with severe matrix disruption had significant myofibroblast presence, scar grade 3, see Table 1.

A panel of extracellular matrix components was chosen to further evaluate matrix organization, tissue and basement membrane regeneration and angiogenesis. Second harmonic generation imaging was also an ideal means of evaluating changes in hierarchical organization. It also provided a more comprehensive assessment of the changes in the injured matrix.

We found some variation in the severity of matrix disorganization within the models of stromal injury. Such variation in wound healing is expected even within a homogeneous population of animals given normal biologic disparities. What factors go into creating these variations is not well understood. One contributing factor is the unavoidable minimal variation in surgical technique, even when surgeries are performed by the same surgeon using a standardized protocol. Infinitesimal differences can exist in even the strictest of inbred animals that result in dissimilar responses to injury.

Why were the burr and burr/keratotomy surgical technique models more effective in creating a desirable scar? [18,30] We hypothesize that a combination of events occurred. First, disruption of basement membrane [31] combined with loss of normal corneal structural integrity and loss of tensile strength were created by the stromal cut. This activates an inflammatory and repair response that resulted in scar. Interestingly, a single partial thickness keratotomy incision was not enough to induce scar formation. We also think that the two techniques described in this manuscript are relevant models akin to injuries from trauma.

The technique used in this study to create scars and to grade these alterations has limitations. A sophisticated custom-made blade was needed to create a partial keratotomy and avoid perforation in these thin corneas. Technically, practice was required to reliably apply force to the cornea during stromal debridement to create scars consistently. Finally, the relevant techniques described in this manuscript add to multiple mechanisms of injury that cause stromal scars, but the findings extrapolated from this technique does not necessarily correspond to any specific type of corneal injury. The modified Fantes grading system we propose is simple and easy to adopt by other researchers. It adds to other classification systems but does not take into consideration the use of sophisticated imaging technologies that incorporate other scar parameters like depth of involvement.

In conclusion, we describe a mouse model of corneal stromal injury that simulates common forms of scar found in clinical practice after severe corneal injury. In our models, the severity of scar density as graded by 2 independent observers often is associated with greater stromal matrix disorganization and cellular infiltration.

Proprietary interests

None.

Acknowledgments

Ambuj Kumar MD, Director of Biostatistics core, University of South Florida collaborated in the statistical design of this manuscript.

This study was supported by NIH/NEI grant EY029395 to EME and an unrestricted grant from the Department of Ophthalmology, Morsani College of Medicine, University of South Florida.

References

[1]. Maurice DM. The structure and transparency of the cornea. J Physiol 1957;136:263–86. [PubMed: 13429485]

[2]. Hassell JR, Birk DE. The molecular basis of corneal transparency. Exp Eye Res 2010;91:326–35. [PubMed: 20599432]

[3]. Meek KM, Knupp C. Corneal structure and transparency. Prog Retin Eye Res 2015;49:1–16. [PubMed: 26145225]

[4]. Espana EM, Birk DE. Composition, structure and function of the corneal stroma. Exp Eye Res 2020;198:108–37.

[5]. Edelhauser HF. The balance between corneal transparency and edema: the Proctor Lecture. Invest Ophthalmol Vis Sci 2006;47:1754–67. [PubMed: 16638979]

[6]. Poole CA, Brookes NH, Clover GM. Keratocyte networks visualised in the living cornea using vital dyes. J Cell Sci 1993;106(Pt 2):685–91. [PubMed: 8282773]

[7]. Tan DT, Dart JK, Holland EJ, Kinoshita S. Corneal transplantation. Lancet 2012;379:1749–61. [PubMed: 22559901]

[8]. Stepp MA, Zieske JD, Trinkaus-Randall V, Kyne BM, Pal-Ghosh S, Tadvalkar G, et al. Wounding the cornea to learn how it heals. Exp Eye Res 2014;121:178–93. [PubMed: 24607489]

[9]. Mohler W, Millard AC, Campagnola PJ. Second harmonic generation imaging of endogenous structural proteins. Methods 2003;29:97–109. [PubMed: 12543075]

[10]. Zipfel WR, Williams RM, Christie R, Nikitin AY, Hyman BT, Webb WW. Live tissue intrinsic emission microscopy using multiphoton-excited native fluorescence and second harmonic generation. Proc Natl Acad Sci U S A 2003;100:7075–80. [PubMed: 12756303]

[11]. Morishige N, Petroll WM, Nishida T, Kenney MC, Jester JV. Noninvasive corneal stromal collagen imaging using two-photon-generated second-harmonic signals. J Cataract Refract Surg 2006;32:1784–91. [PubMed: 17081858]

[12]. Farid M, Morishige N, Lam L, Wahlert A, Steinert RF, Jester JV. Detection of corneal fibrosis by imaging second harmonic-generated signals in rabbit corneas treated with mitomycin C after excimer laser surface ablation. Invest Ophthalmol Vis Sci 2008;49:4377–83. [PubMed: 18502995]

[13]. Kivanany PB, Grose KC, Tippani M, Su S, Petroll WM. Assessment of corneal stromal remodeling and regeneration after photorefractive keratectomy. Sci Rep 2018;8:12580. [PubMed: 30135552]

[14]. Hochheimer BF. Second harmonic light generation in the rabbit cornea. Appl Optic 1982;21:1516–8.

[15]. Bonnans C, Chou J, Werb Z. Remodelling the extracellular matrix in development and disease. Nat Rev Mol Cell Biol 2014;15:786–801. [PubMed: 25415508]

[16]. Ishizaki M, Shimoda M, Wakamatsu K, Ogro T, Yamanaka N, Kao CW, et al. Stromal fibroblasts are associated with collagen IV in scar tissues of alkali-burned and lacerated corneas. Curr Eye Res 1997;16:339–48. [PubMed: 9134323]

[17]. Garana RM, Petroll WM, Chen WT, Herman IM, Barry P, Andrews P, et al. Radial keratotomy. II. Role of the myofibroblast in corneal wound contraction. Invest Ophthalmol Vis Sci 1992;33:3271–82. [PubMed: 1428702]

[18]. Basu S, Hertsenberg AJ, Funderburgh ML, Burrow MK, Mann MM, Du Y, et al. Human limbal biopsy-derived stromal stem cells prevent corneal scarring. Sci Transl Med 2014;6. 266ra172.

[19]. Newman PJ, Berndt MC, Gorski J, White GC 2nd, Lyman S, Paddock C, et al. PECAM-1 (CD31) cloning and relation to adhesion molecules of the immunoglobulin gene superfamily. Science 1990;247:1219–22. [PubMed: 1690453]

[20]. Wynn TA, Vannella KM. Macrophages in tissue repair, regeneration, and fibrosis. Immunity 2016;44:450–62. [PubMed: 26982353]

[21]. Jester JV, Petroll WM, Barry PA, Cavanagh HD. Expression of alpha-smooth muscle (alpha-SM) actin during corneal stromal wound healing. Invest Ophthalmol Vis Sci 1995;36:809–19. [PubMed: 7706029]

[22]. Jester JV, Petroll WM, Cavanagh HD. Corneal stromal wound healing in refractive surgery: the role of myofibroblasts. Prog Retin Eye Res 1999;18:311–56. [PubMed: 10192516]

[23]. Fantes FE, Hanna KD, Waring GO 3rd, Pouliquen Y, Thompson KP, Savoldelli M. Wound healing after excimer laser keratomileusis (photorefractive keratectomy) in monkeys. Arch Ophthalmol 1990;108:665–75. [PubMed: 2334323]

[24]. Hanna KD, Pouliquen YM, Savoldelli M, Fantes F, Thompson KP, Waring GO 3rd, et al. Corneal wound healing in monkeys 18 months after excimer laser photorefractive keratectomy. Refract Corneal Surg 1990;6:340–5. [PubMed: 2257258]

[25]. SundarRaj N, Geiss MJ 3rd, Fantes F, Hanna K, Anderson SC, Thompson KP, et al. Healing of excimer laser ablated monkey corneas. An immunohistochemical evaluation. Arch Ophthalmol 1990;108:1604–10. [PubMed: 1700895]

[26]. Hanna KD, Pouliquen YM, Waring GO 3rd, Savoldelli M, Fantes F, Thompson KP. Corneal wound healing in monkeys after repeated excimer laser photorefractive keratectomy. Arch Ophthalmol 1992;110:1286–91. [PubMed: 1520118]

[27]. Hemmavanh C, Koch M, Birk DE, Espana EM. Abnormal corneal endothelial maturation in collagen XII and XIV null mice. Invest Ophthalmol Vis Sci 2013;54:3297–308. [PubMed: 23599329]

[28]. Joshi V, Vaishnavi KS, Ojha SK, Singh V, Basu S. A reliable animal model of corneal stromal opacity: development and validation using in vivo imaging. Ocul Surf 2020.

[29]. Mohan RR, Stapleton WM, Sinha S, Netto MV, Wilson SE. A novel method for generating corneal haze in anterior stroma of the mouse eye with the excimer laser. Exp Eye Res 2008;86:235–40. [PubMed: 18068702]

[30]. Singh V, Torricelli AA, Nayeb-Hashemi N, Agrawal V, Wilson SE. Mouse strain variation in SMA(+) myofibroblast development after corneal injury. Exp Eye Res 2013;115:27–30. [PubMed: 23791965]

[31]. Wilson SE, Marino GK, Torricelli AAM, Medeiros CS. Injury and defective regeneration of the epithelial basement membrane in corneal fibrosis: a paradigm for fibrosis in other organs? Matrix Biol 2017;64:17–26. [PubMed: 28625845]

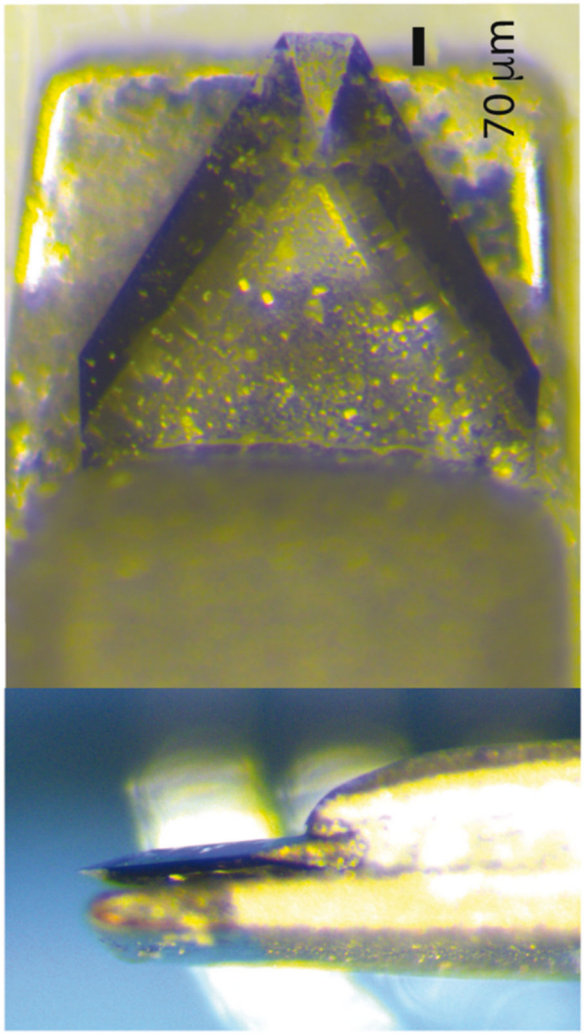

Fig. 1.

A custom-made diamond blade with 70 µm guarded depth to avoid stromal perforation was used in these experiments.

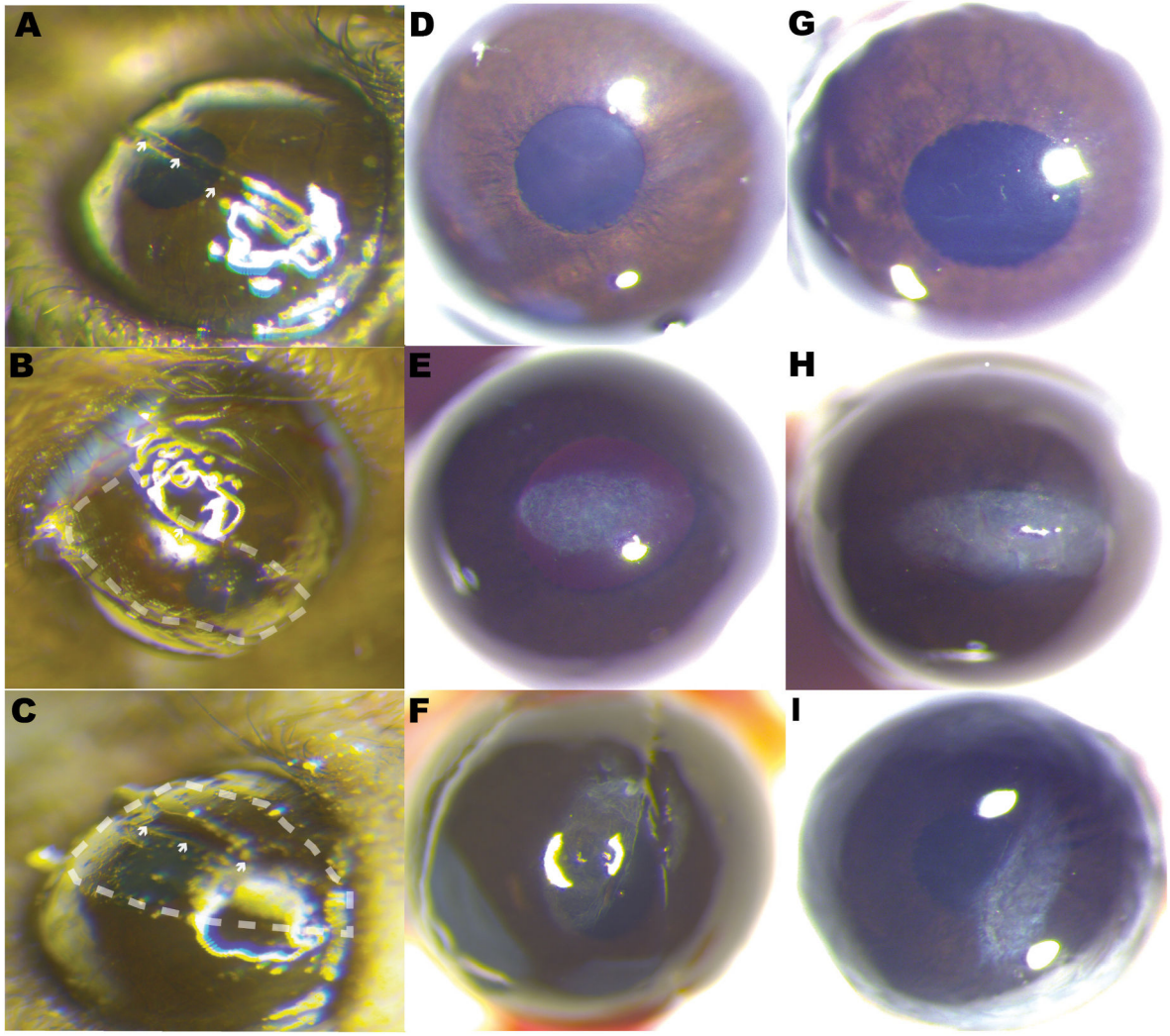

Fig. 2.

Photographs illustrate different surgical techniques used to induce scar formation. A horizontal cut, technique 1 (A), horizontal abrasion into the stroma, technique 2 (B), and central cut and abrasion on both sides, technique 3 (C). Dash lines symbolize abrasion to the stroma with an AlgerBrush II burr. Arrowheads show keratotomy. Scar formation in the three surgical injury models studied. Different examples of scar tissue obtained by a horizontal cut into the stroma, technique 1 (D and G), horizontal abrasion technique 2 (E and H), and central cut and abrasion on both sides, technique 3 (F and I).

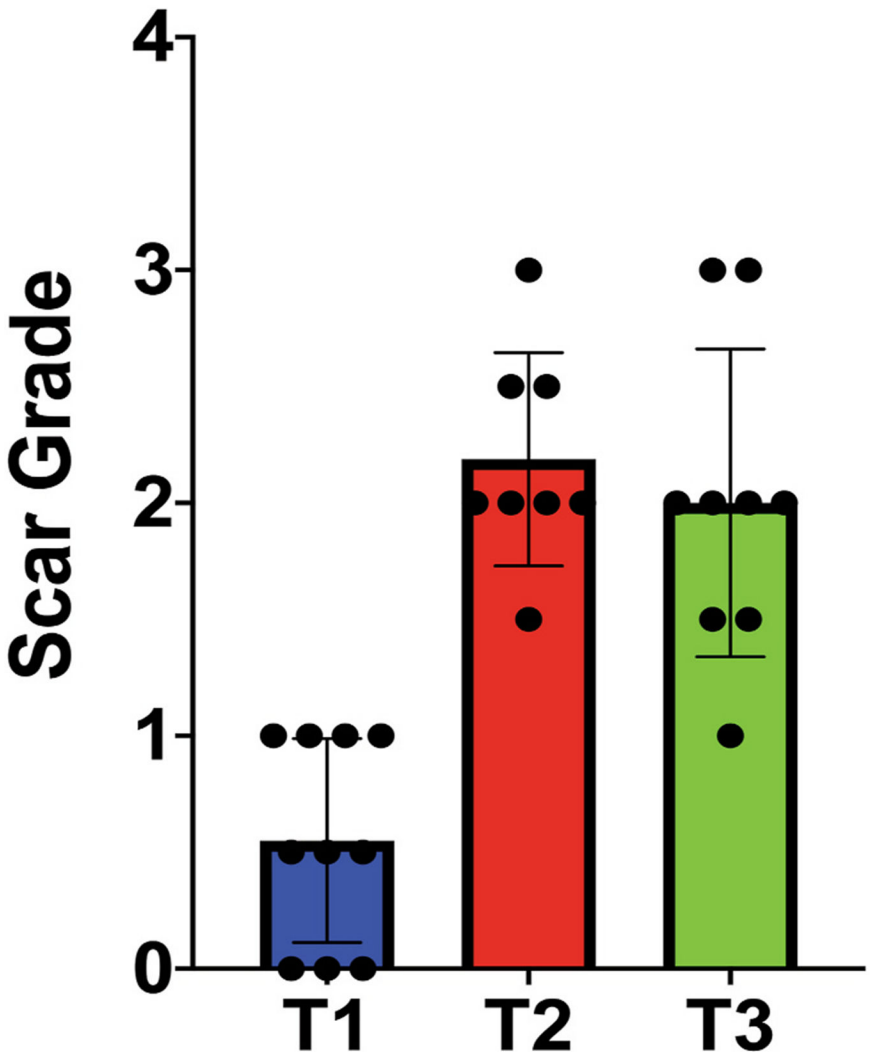

Fig. 3.

Plot shows differences in scar formation between the three different techniques. T1: partial keratotomy, T2: horizontal abrasion only, T3: central cut and abrasion on both sides.

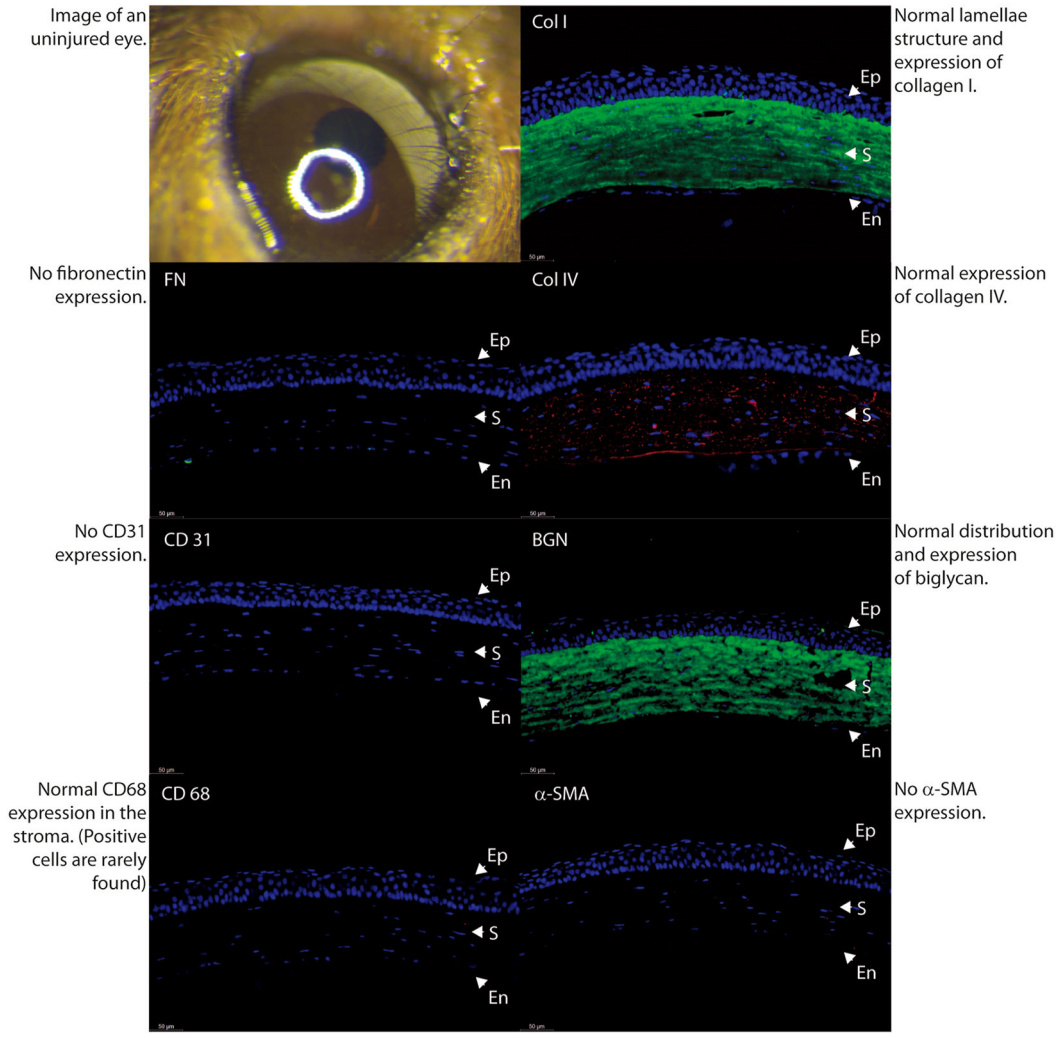

Fig. 4.

Comparison of stromal matrix organization, neovascularization and macrophage infiltration in a normal uninjured adult eye.

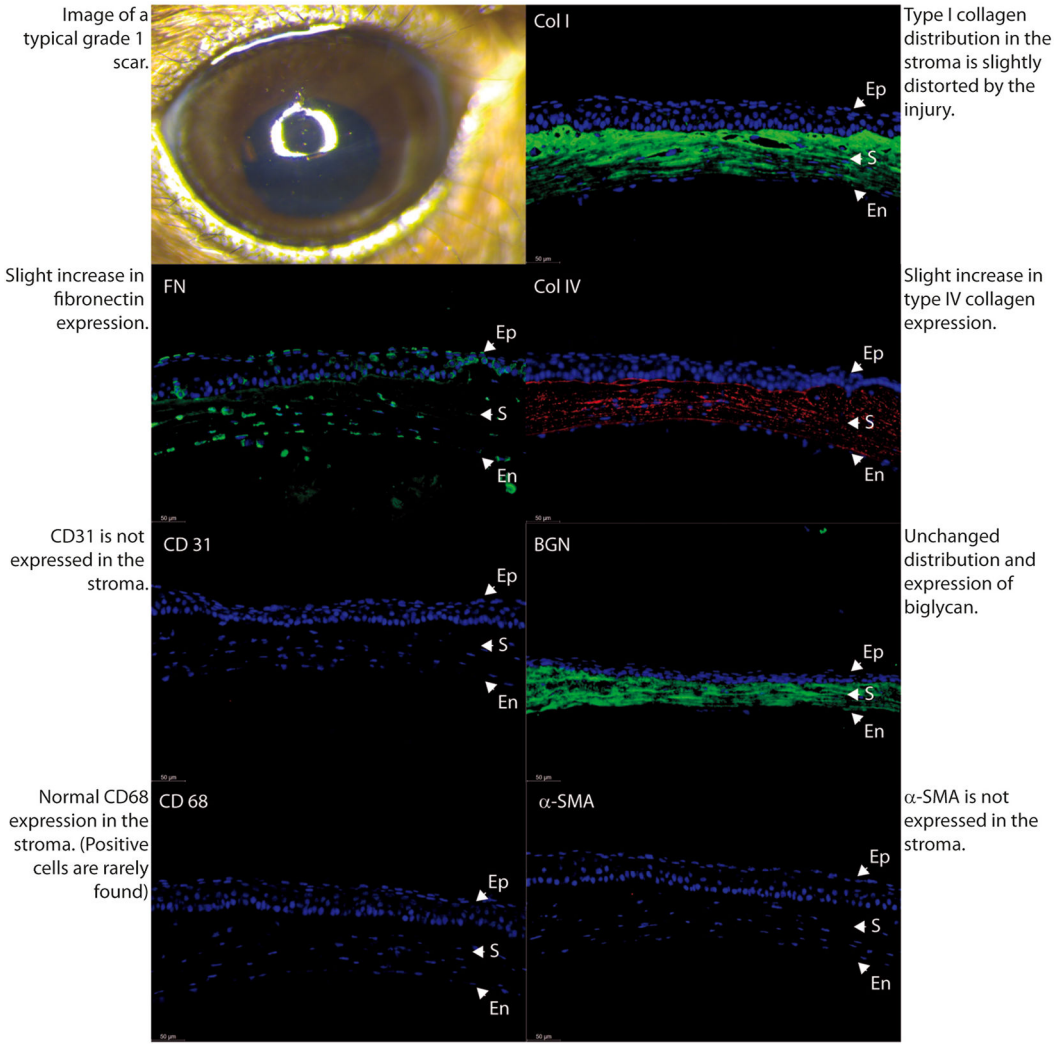

Fig. 5.

Comparison of stromal matrix organization, neovascularization and macrophage infiltration in an eye classified by masked examiner as mild scar, grade 0.

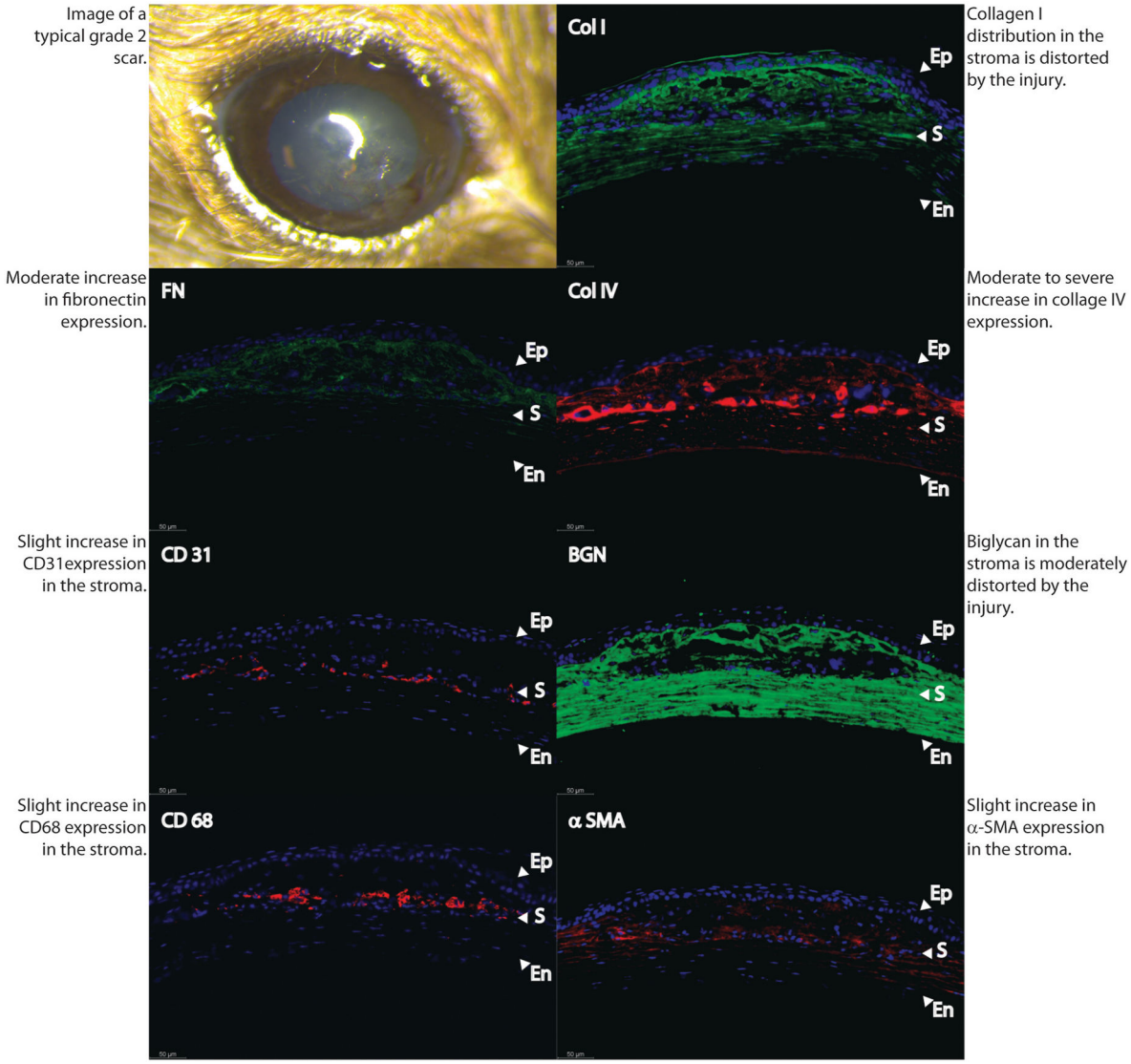

Fig. 6.

Differences in stromal matrix organization, neovascularization and macrophage infiltration become more notorious between an eye classified as grade 1.

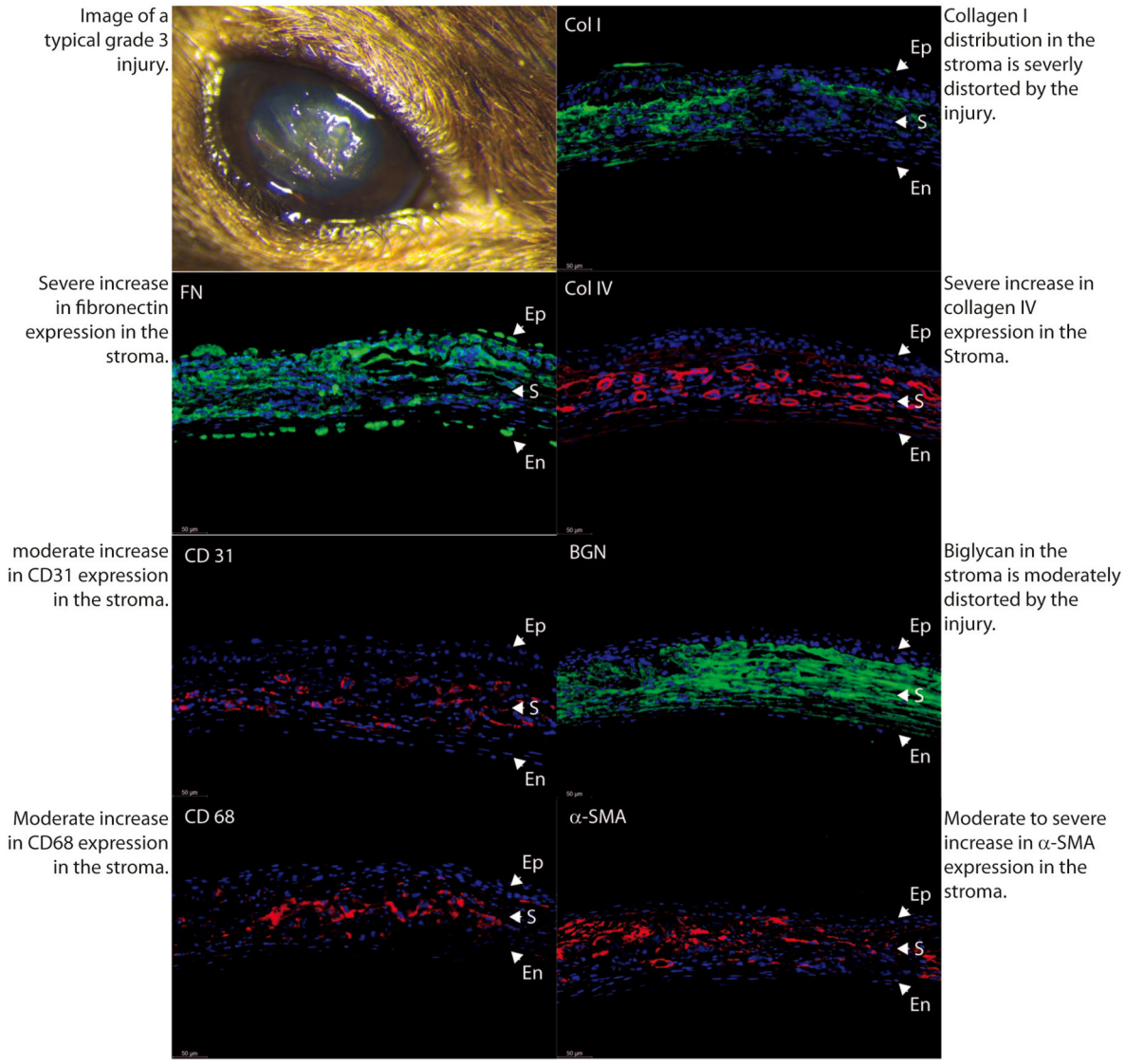

Fig. 7.

Poor stromal matrix organization, significant neovascularization and macrophage infiltration in an eye classified by masked examiner as severe scar, (Grades 2 and 3).

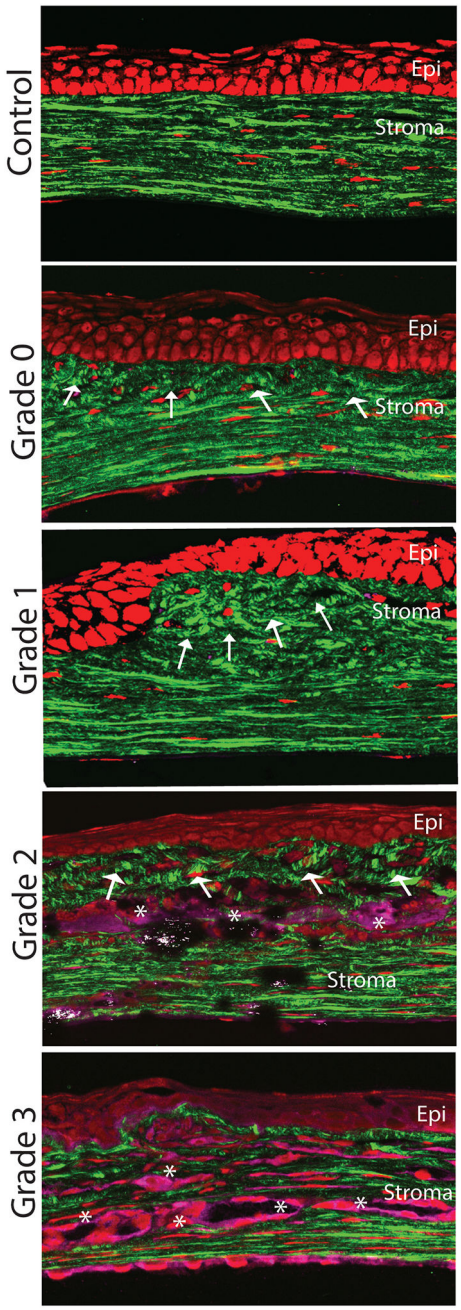

Fig. 8.

Changes in stromal organization in scars of different severity. Normal well-organized matrix and keratocytes (control normal stroma). More prominent matrix disorganization mostly localized to the anterior stroma noted in mild and moderate scars (Grades 0 and 1). Progressive worsening in matrix organization, cellular infiltration and neovascularization in more dense scars (Grades 2 and 3). Arrows show lamellae organization and asterisks presumed neovascularization.

Table 1

Histological characterization of corneal scars graded based on slit lamp microphotographs classification by masked examiners.

Stromal Scar Grade						
	Fibronectin	**Collagen IV**	**CD31**	**CD68**	**α-SMA**	**Fantes modified**
Grade 0	−	−	−	Very rare	−	Trace haze seen with careful oblique illumination.
Grade 1	+	−		Rare	−	Noticeable haze not interfering with visibility of fine iris details, haze smaller than ¼ corneal area. No neovessels.
Grade 2	++	+	+	+	+	Mild obscuration of iris details and haze larger than ¼ corneal area with or without neovascularization.
Grade 3	+++	++	++	++	++	Obscuration of the iris and lens with or without neovascularization.

Ocul Surf. Author manuscript; available in PMC 2022 January 01.